Organic Electronics 76 (2020) 105450

Contents lists available at ScienceDirect

Organic Electronics

journal homepage: www.elsevier.com/locate/orgel

Photocurrent deviation from linearity in an organic photodetector due to limited hole transport layer conductivity

J. Euvrard[a], A. Revaux[a,*], A. Kahn[b], D. Vuillaume[c]

[a] Univ. Grenoble Alpes, CEA-LITEN, Grenoble, 38000, France
[b] Dept. of Electrical Engineering, Princeton University, Princeton, NJ, 08544, USA
[c] IEMN, CNRS, Univ. Lille, Villeneuve d'Ascq, 59652, France

ARTICLE INFO

Keywords:
Organic photodetectors
Organic semiconductor doping
Photocurrent linearity

ABSTRACT

It has been demonstrated that p-doped polymer layers are a convenient replacement as hole transport layer (HTL) for the widely used Poly(3,4-ethylenedioxythiophene)-poly(styrenesulfonate) (PEDOT:PSS), yielding comparable photodetection performances at low light intensities. In this work, we aim to evaluate the response of organic photodetectors (OPDs) with increasing light intensity when p-doped PBDTTT-c is used as HTL. Photocurrent linearity measurements are performed on devices processed with both PEDOT:PSS and p-doped PBDTTT-c to better determine the role of the HTL. We show a deviation of the photocurrent from linearity for light intensities above 10^{-3} W/cm^2 at 0 V applied bias due to distinct mechanisms depending on the HTL material. While space charge limited photocurrent (SCLP) explains the non-linearity at high light intensity for the device processed with PEDOT:PSS, bimolecular recombination is responsible for the loss in linearity when p-doped PBDTTT-c is used as HTL. The replacement of PEDOT:PSS by p-doped PBDTTT-c, which is 6 orders of magnitude less conductive, induces Langevin recombination, causing photocurrent non-linearity. Therefore, this study emphasizes the need for highly conductive transport layers when photodetection applications are targeted, and motivates further improvements in organic semiconductor doping.

1. Introduction

Organic photodetectors (OPDs) arose with the emergence of organic small molecules and polymers benefiting from semiconducting properties [1]. OPDs target applications in imaging and optical communication [2,3] with the advantage of being solution processable at low temperature and on large area [4]. Resulting devices can be produced on light, flexible and transparent substrates such as glass, plastic or paper.

Although OPDs have achieved performances that are competitive with those of their silicon-based counterparts [1,5], their instability in ambient environment, including oxygen and humidity, and under UV radiation and temperature is problematic, and needs to be addressed to allow large-scale industrialization [6–8]. Poly(3,4-ethylenedioxythiophene)-poly(styrenesulfonate) (PEDOT:PSS) used as hole transport layer (HTL) in organic photodetectors and solar cells has been identified as responsible for several degradation mechanisms due to its sensitivity to humidity, oxygen and UV radiation [9–11].

The replacement of PEDOT:PSS by a p-doped organic layer deposited by lamination was introduced by Dai et al. [12] in organic solar cells. Moreover, in a previous study [13] we replaced the PEDOT:PSS HTL by a p-doped polymer layer in OPDs. Replacing PEDOT:PSS by poly[(4,8-bis-(2-ethylhexyloxy)-benzo(1,2-b-4,5-b0)dithiophene)-2,6-diylalt-(4-(2-ethylhexanoyl)-thieno[3,4-b]thiophene-)-2-6-diyl)] (PBDTTT-c) p-doped with tris-[1-(trifluoroethanoyl)-2-(trifluoromethyl)ethane-1,2-dithiolene (Mo(tfd-COCF$_3$)$_3$) leads to similar current-density J(V) and external quantum efficiency (EQE) characteristics at light intensity around 6.5×10^{-5} W/cm^2. However, photodetectors need to cover a wide range of light intensities with constant responsivity, and therefore photocurrent linearity, to be used for imaging applications [14,15]. In this study, we evaluate the ability of photodetectors with p-doped polymer as HTL to respond to variable light intensities and establish the requirements to ensure photocurrent linearity. The role of the HTL is de-coupled from the impact of the active layer and electron transport layer (ETL) by analyzing the photocurrent linearity with PEDOT:PSS as HTL.

2. Experimental methodology

An inverse structure is used in this study with two different HTLs.

* Corresponding author.
E-mail address: amelie.revaux@cea.fr (A. Revaux).

https://doi.org/10.1016/j.orgel.2019.105450
Received 6 May 2019; Received in revised form 10 September 2019; Accepted 10 September 2019
Available online 13 September 2019
1566-1199/

The diodes are processed on indium tin oxide (ITO) coated glass substrates, with patterned electrodes defined by photolithography. To adjust the cathode work function, polyethylenimine (PEIE) is spin-coated on ITO, annealed at 100 °C and rinsed with deionized water. A 500 ± 20 nm thick PBDTTT-c:C_{60}-PCBM active layer with a 1:1.5 ratio in weight is then spin-coated on ITO/PEIE. The thickness of the layers is measured using a contact profilometer. To optimize the bulk heterojunction morphology, the polymer and fullerene are dissolved in chlorobenzene (CB):trichlorobenzene (TCB) with a 90:10 ratio in volume [16]. The solution is stirred for 12 h at 45 °C and filtered at 0.2 µm before deposition. The resulting layer is annealed at 115 °C under nitrogen for 15 min. The HTL, 180 ± 10 nm thick PEDOT:PSS or 45 ± 10 nm thick 5% p-doped PBDTTT-c, is then deposited on the active layer. The thickness of the PEDOT:PSS layer has been optimized to obtain similar injection current density in the dark and similar External Quantum Efficiency for both PEDOT:PSS and p-doped polymer HTL layers [13]. A soft contact transfer lamination (SCTL) is required to deposit the doped layer without dissolving the active layer [12]. Therefore, we also use SCTL for the PEDOT:PSS deposition to ensure a good comparison between the two devices. The technique described by Gupta et al. [17] is used to deposit PEDOT:PSS by lamination and the SCTL technique developed to deposit organic layers was described by Dai et al. [12]. The PEDOT:PSS thickness optimization was detailed in a previous study [13]. Finally, a 100 nm thick aluminum electrode is evaporated through a shadow mask in a vacuum chamber and the devices are encapsulated with glass in the glovebox using an epoxy glue. The current density versus voltage curves for the two diodes studied in this work are shown in supplementary information (Fig. S1).

Current-voltage measurements are carried out using a Keithley 2636A source meter. A halogen lamp is used as light source and the light intensity is varied from 10^{-7} to 10^{-1} W/cm^2 (approximately 1 Sun AM1.5) with optical density filters. Details about the measurement uncertainty are given in supplementary information.

3. Results and discussion

In order to determine the photocurrent linearity of OPDs, we measure the photocurrent for different light intensities at a given applied bias. A power law is used to describe the photocurrent J_{ph} dependence on light intensity P_{light}: $J_{ph} \propto P_{light}^{\alpha}$. When only monomolecular recombination occurs in the active layer, the coefficient α is close to unity [18–20]. Monomolecular recombination includes all processes where the recombination rate depends on n or p, where n and p are the electron and hole carrier densities, respectively [21]. As a result, trap assisted recombination described by Shockley-Read-Hall model is monomolecular for bulk and interface traps [22,23]. On the other hand, bimolecular recombination necessarily involves an electron and a hole [23]. Therefore, the evolution of the recombination rate depends on the product np and increases with the light intensity, leading to $\alpha < 1$. Bimolecular recombination is often described by the Langevin formalism with the bimolecular recombination rate R_B given by the following equation:

$$R_B = \gamma_r (np - n_i^2), \quad (1)$$

with γ_r is the bimolecular recombination rate constant and n_i the intrinsic carrier density. The validity of Langevin theory in organic solar cells has been discussed in the literature, raising doubts regarding the determination of γ_r [23]. However, the nature of γ_r has no impact on the coefficient α. For a device in which recombination is mostly bimolecular, the constant α approaches 0.5 when the applied bias approaches V_{OC} [18]. For most solar cells and photodiodes, both monomolecular and bimolecular recombination compete, resulting in a constant α varying from 0.5 to 1. The loss of photocurrent linearity at high light intensity can also be described by the formation of a space charge region at one interface and is called space charge limited photocurrent (SCLP) leading to $\alpha = 0.75$ [24]. This phenomenon arises when the extraction of one type of carrier is less efficient than the other. As good photocurrent linearity with light intensity is required for photodetection applications, bimolecular recombination and SCLP need to be reduced or suppressed.

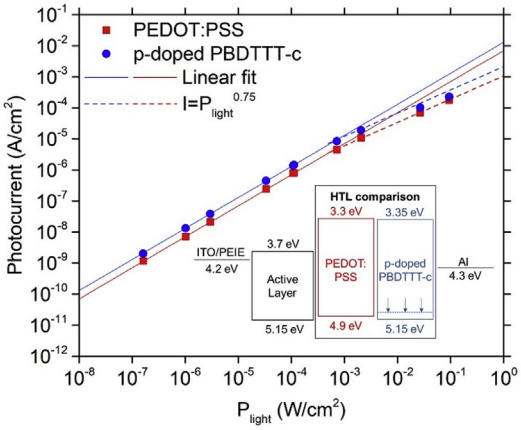

Fig. 1. Linearity measurements of the photocurrent at 0 V with respect to light intensity for the diodes with PEDOT:PSS (red) and p-doped PBDTTT-c (blue) as HTL. A linear and 3/4 power law fits are added to the graph and a band diagram of the structure is given as inset. (For interpretation of the references to colour in this figure legend, the reader is referred to the Web version of this article.)

The photocurrent measurements at 0 V for the diodes with PEDOT:PSS and p-doped PBDTTT-c are shown in Fig. 1. To verify the photocurrent linearity of the diodes with respect to light intensity, a linear fit is added to the graph. We notice a deviation from linearity for light intensities above 10^{-3} W/cm^2, with a slightly stronger deviation when the p-doped polymer is used as HTL. We have verified the reproducibility of the linearity deviation measuring 3 different devices for each HTL material (Fig. S2 in supplementary information). Although linearity is commonly verified in the reverse bias regime, electrical transport weaknesses are highlighted when no potential is applied to the device. To identify and understand the origin of the linearity deviation for each device, we investigate both SCLP and bimolecular recombination hypotheses.

The formation of a space charge region can be due to unbalanced electron and hole mobilities or an extraction barrier at an electrode [25]. The OPD processed in this study should not exhibit extraction barriers as the work function of PEIE-coated ITO is higher than the blend electron affinity, and p-doped PBDTTT-c and PEDOT:PSS exhibit sufficient and similar injection and extraction capabilities, as shown in a previous study [13]. The hole mobility μ_h of PBDTTT-c has been measured around $6 \times 10^{-4}\ cm^2V^{-1}s^{-1}$ [26], while an electron mobility μ_e of $2 \times 10^{-3}\ cm^2V^{-1}s^{-1}$ has been reported for C_{60}-PCBM [27]. Therefore, we can assume that a non-negligible effect results from imbalanced mobilities in the PBDTTT-C:$_{60}$-PCBM active layer at low electric field obtained with applied biases between V_{OC} and 0 V, leading to SCLP.

In order to determine whether the photocurrent deviation from linearity is caused by SCLP, we derive the photocurrent dependence on light intensity as shown by Mihailetchi et al. [24]. Assuming $\mu_h < \mu_e$ in the PBDTTTc:C_{60}-PCBM active layer, we consider $L_e > L_h$ and assume $L_h < w$ where L_e and L_h are the electron and hole mean free paths and w is the active layer thickness. The mean free path in organic semiconductors usually ranges from 0.1 to 10 nm [28]. Therefore, with a 500 nm thick active layer, the assumption $L_h < w$ is reliable.

If holes have a lower mobility than electrons, they will accumulate at the anode interface as their mean free path is reduced compared to electrons. In order to satisfy Poisson's equation, the potential distribution in the active layer is modified with the formation of a band bending near the anode interface. A space charge region is therefore created in the active layer extending over a length L_1 with a voltage drop V_1, as

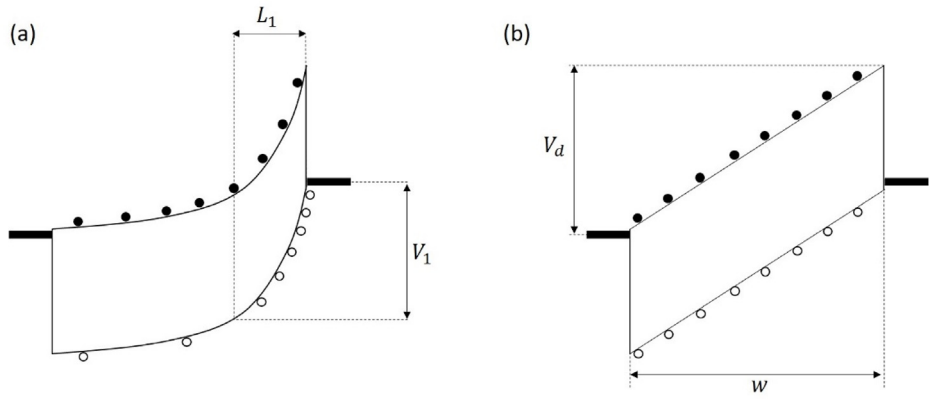

Fig. 2. Schematic of the energy band diagram for the photodetector under illumination in reverse bias (a) when a space charge is formed at the anode side of the active layer and (b) when the electric field is constant in the device.

shown in the schematic given in Fig. 2 (a). Fig. 2 (b) exhibits a band diagram considering a constant electric field in the device. In this latter case, no charge accumulation is created at the interface.

Goodman and Rose have shown that for $\mu_n\tau_n \ll \mu_p\tau_p$, the active layer can be divided into two parts: the space charge region of length L_1 with a voltage drop V_1 where most of the photocurrent is generated and a second part of length $w - L_1$ and zero electric field where the generation and recombination rates are equal [29]. Considering that almost the entire voltage drop V_d is located in the space charge region, $V_d = V_1$, the photocurrent J_{ph} is given by the following equation when holes are the limiting carriers [24].

$$J_{ph} = qGL_1 = qG\sqrt{\mu_h\tau_h}\sqrt{V_d}, \tag{2}$$

where q is the elementary charge, G the electron-hole optical generation rate and τ_h the hole lifetime. Goodman and Rose [29] explain that the space charge region impact is given by the difference between the effective photocurrent and the maximum photocurrent permitted in the active layer. The space charge limited current J_{SCL} in the space charge region when holes are the limiting carriers is given by the following relation [24].

$$J_{SCL} = \frac{9}{8}\varepsilon_0\varepsilon_r\mu_h\frac{V_1^2}{L_1^3}, \tag{3}$$

where ε_0 and ε_r are the vacuum and relative permittivities, respectively. A condition on the length of the space charge region L_{max} required to observe SCLP is obtained when $J_{ph} = J_{SCL}$. When the length of the space charge region reaches L_{max}, the photocurrent is described by the following relation [24].

$$J_{ph} = q\left(\frac{9\varepsilon_0\varepsilon_r\mu_h}{8q}\right)^{1/4} G^{3/4}\sqrt{V_d} \tag{4}$$

We observe that the photocurrent exhibits a square root dependence on the applied bias. Fig. S3 in supplementary information shows the photocurrent J_{ph} with respect to $V_0 - V = V_d$ where V_0 is the potential at which $J_{ph} = 0$. We observe the appearance of a square root regime at light intensities above $2.1 \times 10^{-3}\ W/cm^2$ and $1.1 \times 10^{-4}\ W/cm^2$ for the diodes with PEDOT:PSS and p-doped PBDTTT-c, respectively. However, this square root evolution on its own cannot prove the formation of a space charge region as a similar trend is observed when the photocurrent is limited by the mobility-lifetime product described in equation (2) [24]. We can identify the origin of the square root evolution and determine whether SCLP leads to a non-linear photocurrent dependency with the generation rate G. In our structure, we can consider that $G \propto P_{light}$ [24]. This assumption is strengthened by the linear dependency of the photocurrent at lower light intensities. As shown in Fig. 1, a good fit is obtained at 0 V with $J \propto P_{light}^{3/4}$ above 10^{-3} W/cm^2 for the diode processed with PEDOT:PSS as HTL.

However, with the p-doped PBDTTT-c layer replacing PEDOT:PSS, the high light intensity photocurrent deviates from the ¾ power law, casting doubt on whether SCLP alone can explain the deviation from linearity (Fig. 1). To further probe this issue, we measured the photocurrent vs. light intensity for biases above 0 V. When the applied bias

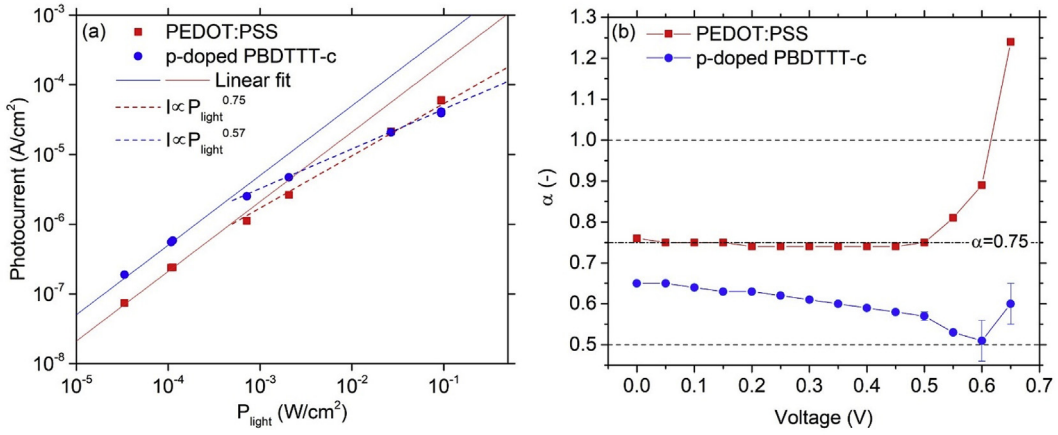

Fig. 3. (a) Photocurrent with respect to light intensity for diodes processed with PEDOT:PSS (red) and p-doped PBDTTT-c (blue) as HTL at 0.5 V. Linear and 3/4 power law fits are added to the graph. (b) Evolution of the α coefficient extracted between 10^{-3} and 10^{-1} W/cm^2 with applied bias ranging from 0 to 0.65 V for the diodes processed with PEDOT:PSS (red) and p-doped PBDTTT-c (blue) as HTL. (For interpretation of the references to colour in this figure legend, the reader is referred to the Web version of this article.)

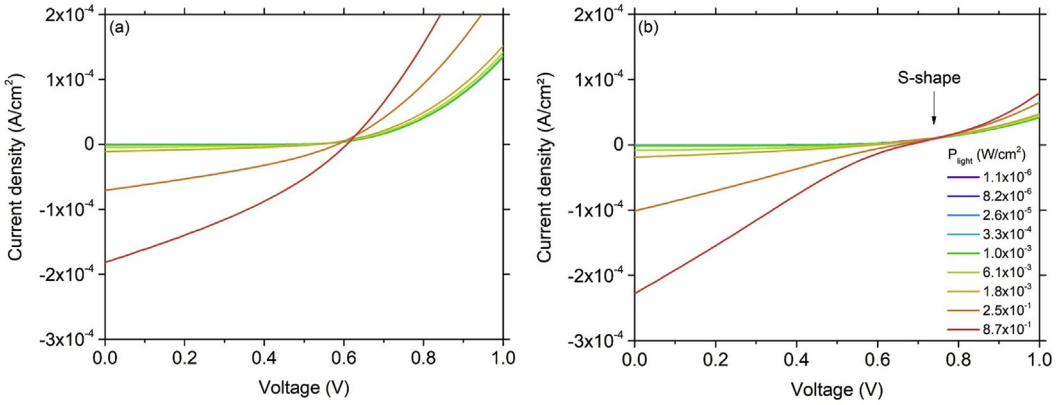

Fig. 4. Current density under illumination with different intensities from 1.1×10^{-6} $\boldsymbol{W/cm^2}$ to 8.7×10^{-1} $\boldsymbol{W/cm^2}$ for the devices processed with PEDOT:PSS (a) and p-doped PBDTTT-c (b) as HTL. The arrow indicates the S-shape formed around V_{OC} at higher light for the device with p-doped polymer as HTL.

increases, the internal electric field is reduced and recombination losses increase [19]. Fig. 3 (a) shows the photocurrent measurements at 0.5 V bias and Fig. S4 in supplementary information displays the photocurrent evolution for an intermediate applied bias of 0.3 V. Although SCLP still explains the linearity deviation for the diode with PEDOT:PSS, the photocurrent of the diode processed with p-doped PBDTTT-c as HTL deviates from the 3/4 power law at high light intensities, and this deviation is emphasized when the internal electric field is reduced, yielding a power law of 0.57 for a bias of 0.5 V. To properly analyze the voltage dependency of the α coefficient, α values were extracted between 10^{-3} and 10^{-1} W/cm^2 for applied biases varying between 0V and V_{OC} (≈0.65–0.7 V) and are summarized in Fig. 3 (b). Between 0 and 0.5 V applied bias, α is constant around 0.75 for the device processed with PEDOT:PSS as HTL, consistent with the SCLP mechanism. On the other hand, α decreases continuously from 0.65 at 0 V to 0.51 at 0.6 V when p-doped PBDTTT-c is used as HTL. A power law decreasing toward 0.5 when the applied bias approaches V_{OC} is characteristic of bimolecular recombination. For both devices, an increase of the α coefficient is observed above 0.5–0.6 V and is attributed to the increasing contribution of diffusion and injection currents [30].

Therefore, while SCLP due to imbalanced mobilities in the bulk heterojunction can explain the loss of linearity in the photocurrent at high light intensity with the PEDOT:PSS HTL, bimolecular recombination dominates for the diode processed with the p-doped PBDTTT-c HTL. As a result, the active layer is no longer limiting the photocurrent linearity when p-doped PBDTTT-c is used as HTL. The main difference between the two HTL materials is their hole conductivity σ_h. The hole conductivity of PEDOT:PSS was measured using the four point probe method at 425 S/cm, while that of a PBDTTT-c layer doped with 5% Mo $(tfd\text{-}COCF_3)_3$ is measured around 10^{-4} S/cm [31]. Although the difference of 6 orders of magnitude is not critical for injection properties as effective barrier lowering has been demonstrated in a previous study [13], it can explain the increase in Langevin recombination. Indeed, a series resistance R_S induces a voltage drop outside the active layer, leading to a reduction of the internal electric field [32], and the probability of bimolecular recombination increases due to higher carrier densities. Street et al. [33] showed that a series resistance equivalent to or above 5 Ωcm^2 reduces significantly the photocurrent density J_{ph}.

To evaluate the impact of the HTL material on the photocurrent density, we estimate the series resistance due to each layer according to $R_S = A/d\sigma_h$, where A is the effective diode area and d the HTL thickness. As a first approximation, series resistance around 5 Ωcm^2 and 10^7 Ωcm^2 are obtained for PEDOT:PSS and p-doped PBDTTT-c HTLs respectively. The high conductivity of PEDOT:PSS provides a sufficiently low series resistance while the limited conductivity of p-doped PBDTTT-c induces a significant series resistance. As R_S of the p-doped polymer HTL is 6 orders of magnitude higher than the threshold value of 5 Ωcm^2, it is likely that the series resistance caused by this layer is responsible for the photocurrent deviation from linearity due to bimolecular recombination.

In order to further investigate this hypothesis, we measured the J(V) characteristics for both photodiodes with varying light intensities. If a series resistance and bimolecular recombination are responsible for the photocurrent decrease, we expect the formation of an S-shape around V_{OC} with increasing light intensity [19,34,35]. Fig. 4 (a) and (b) exhibit the J(V) measurements under different light intensities for the diodes processed with PEDOT:PSS and p-doped polymer, respectively. The J(V) measurements are also given in a semilogarithmic scale in supplementary information (Fig. S5). For light intensities above 10^{-2} W/cm^2, an inflection appears around V_{OC} for the diode with p-doped PBDTTT-c as HTL (a zoom on J(V) at lower light intensities is given in Supplementary Information Fig. S6) while no degradation is observed in the J(V) characteristics when PEDOT:PSS is used as HTL. The appearance of the S-shape with increasing light intensity is consistent with an increased voltage drop in the HTL as the photogenerated current increases [33]. Therefore, this result is consistent with the hypothesis of an insufficient hole conductivity in the p-doped PBDTTT-c layer.

4. Conclusion

In this study we measured and analyzed the OPD response to variable light intensities when the widely used HTL material PEDOT:PSS is replaced by p-doped PBDTTT-c. For both types of devices, a photocurrent deviation from linearity is observed for light intensities above 10^{-3} W/cm^2 at 0 V. Space charge limited photocurrent (SCLP) probably due to imbalanced electron and hole mobilities in the bulk heterojunction is suggested to be responsible for this deviation when PEDOT:PSS is used as HTL, while bimolecular recombination is involved for the device processed with p-doped PBDTTT-c. As photocurrent linearity is required over a wide range of light intensities for imaging applications, solutions need to be provided to improve their performances. SCLP could be avoided by improving the electron mobility to reach balanced mobilities for both types of carriers in the active layer. Motivated by the need for more stable devices, we investigated here p-doped PBDTTT-c as an alternative to PEDOT:PSS. The study shows that the hole conductivity of p-doped PBDTTT-c needs to be increased by several orders of magnitude to avoid voltage drop outside the active layer and limit bimolecular recombination. Although doping leads to a major improvement of organic layer conductivities, a limited doping efficiency is often observed at high doping concentration [36,37]. The origin of this limited doping efficiency for various dopant-semiconductor mixtures is currently studied in the literature [38–42].

Acknowledgments

Work in Princeton was supported by a grant from the National Science Foundation (DMR- 1807797). AK thanks the group of Prof. Seth Marder for providing the dopants.

Appendix A. Supplementary data

Supplementary data to this article can be found online at https://doi.org/10.1016/j.orgel.2019.105450.

References

[1] R.D. Jansen-van Vuuren, A. Armin, A.K. Pandey, P.L. Burn, P. Meredith, Organic photodiodes: the future of full color detection and image sensing, Adv. Mater. 28 (2016) 4766–4802, https://doi.org/10.1002/adma.201505405.
[2] K.J. Baeg, M. Binda, D. Natali, M. Caironi, Y.Y. Noh, Organic light detectors: photodiodes and phototransistors, Adv. Mater. 25 (2013) 4267–4295, https://doi.org/10.1002/adma.201204979.
[3] P. Büchele, M. Richter, S.F. Tedde, G.J. Matt, G.N. Ankah, R. Fischer, M. Biele, W. Metzger, S. Lilliu, O. Bikondoa, J.E. Macdonald, C.J. Brabec, T. Kraus, U. Lemmer, O. Schmidt, X-ray imaging with scintillator-sensitized hybrid organic photodetectors, Nat. Photonics 9 (2015) 843–848, https://doi.org/10.1038/nphoton.2015.216.
[4] A.C. Arias, J.D. MacKenzie, I. McCulloch, J. Rivnay, A. Salleo, Materials and applications for large area electronics: solution-based approaches, Chem. Rev. 110 (2010) 3–24, https://doi.org/10.1021/cr900150b.
[5] X. Gong, M. Tong, Y. Xia, W. Cai, J.S. Moon, Y. Cao, G. Yu, C.-L. Shieh, B. Nilsson, A.J. Heeger, High-detectivity polymer photodetectors with spectral response from 300 nm to 1450 nm, Science 325 (2009) 1665–1667, https://doi.org/10.1126/science.1176706.
[6] H. Cao, W. He, Y. Mao, X. Lin, K. Ishikawa, J.H. Dickerson, W.P. Hess, Recent progress in degradation and stabilization of organic solar cells, J. Power Sources 264 (2014) 168–183, https://doi.org/10.1016/j.jpowsour.2014.04.080.
[7] H. Kang, G. Kim, J. Kim, S. Kwon, H. Kim, K. Lee, Bulk-heterojunction organic solar Cells : five core technologies for their commercialization, Adv. Mater. 28 (2016) 7821–7861, https://doi.org/10.1002/adma.201601197.
[8] W.R. Mateker, M.D. Mcgehee, Progress in understanding degradation mechanisms and improving stability in organic photovoltaics, Adv. Mater. 29 (2017) 1603940, https://doi.org/10.1002/adma.201603940.
[9] K. Norrman, M.V. Madsen, S.a. Gevorgyan, F.C. Krebs, Degradation patterns in water and oxygen of an inverted polymer solar cell, J. Am. Chem. Soc. 132 (2010) 16883–16892, https://doi.org/10.1021/ja106299g.
[10] E. Voroshazi, B. Verreet, A. Buri, R. Müller, D. Di Nuzzo, P. Heremans, Influence of cathode oxidation via the hole extraction layer in polymer:fullerene solar cells, Org. Electron. Physics, Mater. Appl. 12 (2011) 736–744, https://doi.org/10.1016/j.orgel.2011.01.025.
[11] S.B. Sapkota, M. Fischer, B. Zimmermann, U. Würfel, Analysis of the degradation mechanism of ITO-free organic solar cells under UV radiation, Sol. Energy Mater. Sol. Cells 121 (2014) 43–48, https://doi.org/10.1016/j.solmat.2013.10.021.
[12] A. Dai, Y. Zhou, A.L. Shu, S.K. Mohapatra, H. Wang, C. Fuentes-Hernandez, Y. Zhang, S. Barlow, Y.L. Loo, S.R. Marder, B. Kippelen, A. Kahn, Enhanced charge-carrier injection and collection via lamination of doped polymer layers p-doped with a solution-processible molybdenum complex, Adv. Funct. Mater. 24 (2014) 2197–2204, https://doi.org/10.1002/adfm.201303232.
[13] J. Herrbach, A. Revaux, D. Vuillaume, A. Kahn, P-doped organic semiconductor: potential replacement for PEDOT: PSS in organic photodetectors, Appl. Phys. Lett. 109 (2016) 073301, , https://doi.org/10.1063/1.4961444.
[14] G. Konstantatos, J. Clifford, L. Levina, E.H. Sargent, Sensitive solution-processed visible-wavelength photodetectors, Nat. Photonics 1 (2007) 531–534, https://doi.org/10.1038/nphoton.2007.147.
[15] J.R. Manders, T.H. Lai, Y. An, W. Xu, J. Lee, D.Y. Kim, G. Bosman, F. So, Low-noise multispectral photodetectors made from all solution-processed inorganic semiconductors, Adv. Funct. Mater. 24 (2014) 7205–7210, https://doi.org/10.1002/adfm.201402094.
[16] A. Keawprajak, P. Piyakulawat, A. Klamchuen, P. Iamraksa, U. Asawapirom, Influence of crystallizable solvent on the morphology and performance of P3HT:PCBM bulk-heterojunction solar cells, Sol. Energy Mater. Sol. Cells 94 (2010) 531–536, https://doi.org/10.1016/j.solmat.2009.11.018.
[17] D. Gupta, M.M. Wienk, R. a J. Janssen, Efficient polymer solar cells on opaque substrates with a laminated PEDOT:PSS top electrode, Adv. Energy Mater. 3 (2013) 782–787, https://doi.org/10.1002/aenm.201201061.
[18] L.J.A. Koster, M. Kemerink, M.M. Wienk, K. Maturová, R.A.J. Janssen, Quantifying bimolecular recombination losses in organic bulk heterojunction solar cells, Adv. Mater. 23 (2011) 1670–1674, https://doi.org/10.1002/adma.201004311.
[19] T. Hahn, S. Tscheuschner, F.J. Kahle, M. Reichenberger, S. Athanasopoulos, C. Saller, G.C. Bazan, T.Q. Nguyen, P. Strohriegl, H. Bässler, A. Köhler, Monomolecular and bimolecular recombination of electron–hole pairs at the interface of a bilayer organic solar cell, Adv. Funct. Mater. 27 (2017) 1604906, https://doi.org/10.1002/adfm.201604906.
[20] V. Dyakonov, Electrical aspects of operation of polymer-fullerene solar cells, Thin Solid Films 451–452 (2004) 493–497, https://doi.org/10.1016/j.tsf.2003.11.063.
[21] K.C. Kao, Dielectric Phenomena in Solids, Elsevier, 2004.
[22] S.R. Cowan, a Roy, a J. Heeger, Recombination in polymer-fullerene bulk heterojunction solar cells, Phys. Rev. B. 82 (2010) 245207 245207 10.1103/PhysRevB.82.245207.
[23] G. Lakhwani, A. Rao, R.H. Friend, Bimolecular recombination in organic photovoltaics, Annu. Rev. Phys. Chem. 65 (2014) 557–581, https://doi.org/10.1146/annurev-physchem-040513-103615.
[24] V.D. Mihailetchi, J. Wildeman, P.W.M. Blom, Space-charge limited photocurrent, Phys. Rev. Lett. 94 (2005) 126602, https://doi.org/10.1103/PhysRevLett.94.126602.
[25] R.H. Parmenter, W. Ruppel, Two-carrier space-charge-limited current in a trap-free insulator, J. Appl. Phys. 30 (1959) 1548–1558, https://doi.org/10.1063/1.1734999.
[26] B.X. Dong, B. Huang, A. Tan, P.F. Green, Nanoscale orientation effects on carrier transport in a low-band- gap polymer, J. Phys. Chem. C (2014), https://doi.org/10.1021/jp506374m.
[27] V.D. Mihailetchi, J.K.J. Van Duren, P.W.M. Blom, J.C. Hummelen, R.A.J. Janssen, J.M. Kroon, M.T. Rispens, W.J.H. Verhees, M.M. Wienk, Electron transport in a methanofullerene, Adv. Funct. Mater. 13 (2003) 43–46, https://doi.org/10.1002/adfm.200390004.
[28] H.L. Kwok, Carrier mobility in organic semiconductor thin films, Rev. Adv. Mater. Sci. 5 (2003) 62–66.
[29] A.M. Goodman, A. Rose, Double extraction of uniformly generated electron-hole pairs from insulators with noninjecting contacts, J. Appl. Phys. 42 (1971) 2823–2830, https://doi.org/10.1063/1.1660633.
[30] S.R. Cowan, J. Wang, J. Yi, Y.J. Lee, D.C. Olson, J.W.P. Hsu, Intensity and wavelength dependence of bimolecular recombination in P3HT:PCBM solar cells: a white-light biased external quantum efficiency study, J. Appl. Phys. 113 (2013) 154504, https://doi.org/10.1063/1.4801920.
[31] J. Euvrard, A. Revaux, P.-A. Bayle, M. Bardet, D. Vuillaume, A. Kahn, The formation of polymer-dopant aggregates as a possible origin of limited doping efficiency at high dopant concentration, Org. Electron. 53 (2018) 135–140, https://doi.org/10.1016/j.orgel.2017.11.020.
[32] A. Petersen, T. Kirchartz, T. Wagner, Charge extraction and photocurrent in organic bulk heterojunction solar cells, Phys. Rev. B. 85 (2012) 45208, https://doi.org/10.1103/PhysRevB.85.045208.
[33] R. Street, K.W. Song, S. Cowan, Influence of series resistance on the photocurrent analysis of organic solar cells, Org. Electron. 12 (2011) 244–248, https://doi.org/10.1016/j.orgel.2010.11.012.
[34] W. Tress, S. Corvers, K. Leo, M. Riede, Investigation of driving forces for charge extraction in organic solar cells: transient photocurrent measurements on solar cells showing s-shaped current-voltage characteristics, Adv. Energy Mater. 3 (2013) 873–880, https://doi.org/10.1002/aenm.201200931.
[35] W. Tress, K. Leo, M. Riede, Influence of hole-transport layers and donor materials on open-circuit voltage and shape of I-V curves of organic solar cells, Adv. Funct. Mater. 21 (2011) 2140–2149, https://doi.org/10.1002/adfm.201002669.
[36] K. Walzer, B. Maennig, M. Pfeiffer, K. Leo, Highly efficient organic devices based on electrically doped transport\ layers, Chem. Rev. 107 (2007) 1233–1271, https://doi.org/10.1021/cr050156n.
[37] T. Menke, D. Ray, H. Kleemann, M.P. Hein, K. Leo, M. Riede, Highly efficient p-dopants in amorphous hosts, Org. Electron. Physics, Mater. Appl. 15 (2014) 365–371, https://doi.org/10.1016/j.orgel.2013.11.033.
[38] J. Euvrard, A. Revaux, S.S. Nobre, A. Kahn, D. Vuillaume, Toward a better understanding of the doping mechanism involved in Mo(tfd-COCF3)3 doped PBDTTT-c, J. Appl. Phys. 123 (2018) 225501, https://doi.org/10.1063/1.5029810.
[39] M.L. Tietze, J. Benduhn, P. Pahner, B. Nell, M. Schwarze, H. Kleemann, M. Krammer, K. Zojer, K. Vandewal, K. Leo, Elementary steps in electrical doping of organic semiconductors, Nat. Commun. 9 (2018) 1182, https://doi.org/10.1038/s41467-018-03302-z.
[40] Q. Zhang, X. Liu, F. Jiao, S. Braun, M.J. Jafari, X. Crispin, T. Ederth, M. Fahlman, Ground-state charge transfer for NIR absorption with donor/acceptor molecules: interactions mediated via energetics and orbital symmetries, J. Mater. Chem. C. 5 (2017) 275–281, https://doi.org/10.1039/C6TC04563D.
[41] I. Salzmann, G. Heimel, M. Oehzelt, S. Winkler, N. Koch, Molecular electrical doping of organic semiconductors: fundamental mechanisms and emerging dopant design rules, Acc. Chem. Res. 49 (2016) 370–378, https://doi.org/10.1021/acs.accounts.5b00438.
[42] M.L. Tietze, P. Pahner, K. Schmidt, K. Leo, B. Lüssem, Doped organic semiconductors: trap-filling, impurity saturation, and reserve regimes, Adv. Funct. Mater. 25 (2015) 2701, https://doi.org/10.1002/adfm.201404549.